Copyright © 2009 Tech Science Press SDHM, vol.5, no.1, pp.1-31, 2009

# Frequency Domain based Damage Index for Structural Health Monitoring

**G. Giridhara**[1] **and S. Gopalakrishnan**[2]

**Abstract:** In this paper, a new damage measure in the frequency domain (FDI), which uses the definition of strain energy in the frequency domain, is proposed. The proposed damage index is derived using the definition of frequency domain strain energy. The base line responses and the strain energies are computed using Wavelet Spectral Finite elements, while the strain energies for the damaged structure is computed using four high fidelity experimental responses. The sensitivity of the damage measure in locating cracks of different sizes and orientation is demonstrated on a square plate, the rectangular plate and on a compressor blade.

**Keywords:** Structural Health Monitoring, Wavelet Spectral Finite Element, Damage Index, Frequency Domain Strain Energy.

## 1 Introduction

Structural integrity assessment is an approach to assess whether a structure is fit to withstand the service conditions safely and reliably throughout its lifetime. This requires continuous monitoring of the structures over a long period of time. Most of the monitoring is currently performed off-line through non-destructive evaluation techniques. These techniques are too time consuming and laborious and they do not provide the complete information of certain critical parameters such as damage initiation time, the state of the structure at the time of damage initiation etc. The study involving the determination of the state of the structure using the measured responses is called the Structural Health Monitoring (SHM). SHM has four levels as discussed in [Doebling, Farrar, Prime and Daniel (1996)]. Level 1 confirms the presence of cracks in the structure, Level 2 determines the location, size and orientation of the cracks, Level 3 determines the severity of the cracks present and Level 4 deals with the delay or control of the growth of cracks. The Level 1 and Level 2

[1] Department of Mechanical Engineering, BMS College of Engineering, Banagalore, India 560019.
[2] Corresponding author. E-mail: krishnan@aero.iisc.ernet.in Fax:+91-80-2360-0134. Department of Aerospace Engineering, Indian Institute of Science, Bangalore, India 560012.

in SHM are the most difficult problems that require high fidelity data which are not noise polluted, simplified, yet robust mathematical model, and an accurate damage detection methodology that blends well with the chosen mathematical model.

The main objective of this paper is to predict the location and extent of the damage using the measurements obtained from experimental data. There are many different damage detection techniques reported in the literature [Doebling, Farrar, Prime and Daniel (1996); Sohn, Hemez, Shunk, Stinemates and Nadler (2003); Staszewski, Boller and Tomlinson (2003)]. Most of the earlier studies on damage detection were based on modal measurements, wherein the presence of damage was detected by monitoring the changes in the natural frequencies. This method is not a feasible one if the damage size is very small due to low sensitivity and in addition, it requires baseline measurements. It is quite well known that the strain gradient or curvature measurements are more sensitive to small damage sizes [Pandey, Biswas and Samman (1991); Luo and Hanagud (1997); Lestari (2001); Li, Cheng, Yam and Wong (2002)].

A Damage Index based on curvature was first proposed [Ho and Ewins (1999)], which was found highly susceptible to the noise in the measurement. Strain mode technique for identification of damage locations in plate-like structures [Li, Cheng, Yam and Wong (2002)]. Here, based on the Rayleigh Ritz approach, the strain modal analysis of a damaged plate is performed and strain mode shapes are consequently obtained. Another parameter, which can be used as a curvature measure and can be used to construct a Damage Index, is the Strain Energy parameter. By comparing the strain energies of the structure before and after damage, one can estimate the location of the damage. This approach was used for beam type structures [Kim and Stubbs (2003)] and a similar technique was adopted for plate type structures [Cornwell, Doebling and Farrar (1999)]. Damage localization method using Modal Strain Energy Change is discussed in [Shi, Law and Zhang (1998)]. Most of these techniques were based on modal analysis methods and were performed in the time domain. These modal-based methods are very attractive as they provide information regarding the general state of health of the structure. However, they tend to have limited sensitivity and generally they are not accurate enough to provide detailed information regarding damage type and extent, especially when the damage sizes are small.

Sensitivity of the measurements can be significantly increased by using wave propagation based diagnostics. Guided waves such as Lamb or Rayleigh waves in particular have the capability of traveling relatively long distances within the structure under investigation and show sensitivity to a variety of damage types. Hence, the strain energy based damage index obtained from wave propagation based measurements can indeed give a robust measure on the state of the structure. A wave-based

strain energy index was implemented and successfully applied [Sharma, Ruzzene and Hanagud (2006); Giridhara, Gopalakrishnan, Ruzzene, Hanagud and Sharma (2007)]. The important aspect of this approach is that, its baseline measurements are synthesized directly by under sampling (or decimating) the experimental data. In this paper, we use a similar measure (strain energy), however the analysis is performed in the frequency domain. The base line measurement in this case is obtained by wavelet spectral finite element model, while the damaged model is analyzed using spectral analysis. The main difference is that, unlike the one reported in [Sharma, Ruzzene and Hanagud (2006)], the inertial component of energy is built into the formulation.

Monte Carlo Simulation method for the assessment of Multiple Site Damage (MSD) and detection via Wavelet transforms [Horst (2005)]. [Sekhar ](2008) summarize the different studies on double/multi-cracks and to note the influences, identification methods in vibration structures such as beams, rotors, pipes, etc. And thus this paper brings out the state of the research on multiple cracks effects and their identification. The Residual Error Method is applied to a concrete beam in order to identify and quantify damages in its structure based on the alteration produced by damage in the dynamic properties of structures [ Brasiliano, Souza, Doz and Brito (2008)]. Changes on the dynamic behavior, crack trajectories, peak loads and energy variations were observed during the simulation.

An overview of the computational intelligence methods developed for the structural integrity assessment of aging aircraft structures is discussed [Pidaparti (2006)]. A neural network (NN) model is developed for the analysis and prediction of the mapping between degradation of chemical elements and electrochemical parameters during the corrosion process [Pidaparti and Neblett (2007)]. Eigen value sensitivity equations, derived from first-order perturbation technique for typical infrastructural systems are used and Neural network based damage identification is also demonstrated [Raghuprasad, Lakshmanan, Gopalakrishnan, Muthumani (2008)].

A bi-level damage detection algorithm that utilizes dynamic responses of the structure as input and neural network (NN) as a pattern classifier is presented [Lee and Kim (2007)]. The signal anomaly index (SAI) is proposed to express the amount of changes in the shape of frequency response functions (FRFs) or strain frequency response function (SFRF). SAI is calculated by using the acceleration and dynamic strain responses acquired from intact and damaged states of the structure. A damage index in the form of a vector of Fourier coefficients which is robust and unique for a given damage size and damage location is presented by [Reddy; and Ranjan Ganguli (2007)]. The effect of noise in the mode shape data is considered and it is found that Fourier coefficients provide a useful indication of damage even in the presence of noise. Various damage levels are considered and it is found that higher

modes are needed to detect small amount of damage.

In order to overcome various computational problems like large system size, mesh sensitivity, numerical stability and accuracy in the hp-finite element model for wave scattering, a spectral finite element method (SFEM) has been developed [Gopalakrishnan, Chakraborty and Mahapatra (2007)]. SFEM is used to model wave propagation in damaged structures and proved that spectral approach gives more information and is sufficient for damage detection [Ostachowicz (2008)]. The composite beam is modeled as Timoshenko beam using wavelet based spectral finite element (WSFE) method [Shamsh Tabrez, Mira Mitra and Gopalakrishnan (2007)]. The simulated wave responses are then used as surrogate experimental results to predict degradation using a measure called damage force indicator (DFI) and studied the different environmental conditions in term of relative humidity and at a temperature. Time-frequency analysis of various simulated and experimental signals due to elastic wave scattering from damage are performed using wavelet transform (WT) and Hilbert-Huang transform (HHT) and their performances are compared in context of quantifying the damages using SFEM [Gangadharan, RoyMahapatra, Gopalakrishnan, Murthy, Bhat (2009)].

The effectiveness of wavelet transforms has been shown for detection and monitoring of cracks [Prabhakar, Sekhar and Mohanty (2001)]. An application overview of wavelet in fault diagnosis is given in [Peng and Chu (2004)]. [Chang and Chen (2005)] presented a technique for structure damage detection based on spatial wavelet analysis and estimated both the positions and depths of multi-cracks. Wavelet finite element has also been applied for crack detection [Xuefeng, Zhengjia, Qiang and Yanyang (2005)]. [Chen, Zi, Li and He (2006)] used a dynamic mesh-refinement method (DMRM) for identification of multiple cracks. This is based on the relationship of the natural frequency change ratios with crack parameters in a beam.

[Chasalevris and Papadopoulos (2006)] used unique method of a combination of wavelet and eigenfrequency to solve the inverse problem. This procedure is based on the construction of the contours diagrams of the monitored parameter as a function of two independent variables. Here a combination of wavelets analysis (to find the locations of the cracks) and an analysis of output parameters such as the eigenfrequency change (to find the rest of the identification parameters) is used. Normalized wavelet packets quantifiers are proposed and studied as a new tool for condition monitoring [Yanhui Feng and Fernando Schlindwein (2009)]. The new quantifiers construct a complete quantitative time-frequency analysis: the Wavelet packets relative energy measures the normalized energy of the wavelet packets node; the Total wavelet packets entropy measures how the normalized energies of the wavelet packets nodes are distributed in the frequency domain; the Wavelet

packets node entropy describes the uncertainty of the normalized coefficients of the wavelet packets node.

Damage detection through Damage Force Indicator is reported in [Nag, Roy Mahapatra and Gopalakrishnan (2002); Sreekanth Kumar, Roy Mahapatra, and Gopalakrishnan (2004); Schulz, Naser, Pai and Chung (1998)]. Here, the stiffness of the healthy structure and the measured damage response is used to predict the location of damage. This does not require base line solution and can give the location of very small size cracks even in the presence of noise polluted responses. The major disadvantage of this approach is that it requires many sensor measurements and in its present form can give only the location of flaw and not its extent. This method works very well with Spectral Finite Element as its system size is usually very small. Damage detection based on Damage Force Indicator using reduced order FE models is presented [Gupta, Giridhara and Gopalakrishnan (2008)].

The baseline energy in this work is obtained through Wavelet based Spectral Finite Element formulation. The advantages in using wavelet transform is that, the wavelets have localized nature of basis functions which allow finite domain analysis. These are extensively used to study wave propagation in isotropic[Mitra and Goplakrishnan (2005), (2006), (2006)], composites [Mitra and Goplakrishnan (2006)], anisotropic [Mitra and Goplakrishnan (2008)] and nanocomposite structures [Mitra and Goplakrishnan (2006)]. These elements are free from wrap-around problems and can analyze un-damped finite length structures. The accuracy of simulation is independent of the time window. Initial and/or boundary conditions can be conveniently imposed. In addition, one can also obtain the wave parameters such as the wave numbers and the group speeds can be extracted from the formulation. Wavelet spectral elements also enables measurements of responses at the intermediate locations; which are required in the present analysis, through post processing of the nodal solutions. In summary, Wavelet spectral finite element can be used as an ideal tool to perform wave propagation based analysis.

The energy in the damaged structure is obtained using the spectral solution involving four wave coefficients, which are obtained through four high fidelity measurements. The measurement could be time history of displacement, velocity, acceleration or strain. These measured responses are converted to frequency domain using standard FFT algorithm. The entire structural domain is then split into smaller grids where the responses at these intermediate points are obtained from the four measured responses through post-processing of the spectral solution. One of the assumption made in the analysis is that wave numbers do not change much in the presence of damage. Hence, while computing the energies in the damaged structure, the wave number of healthy structure is used. In the analysis, the choice of four experimental points is critical. In the section 4, examples are given to show the

choice of four experimental points on the overall damage estimation. More details on choice of experimental points are discussed in detail in section 4. We are able to predict the presence of damage, its extent and to limited extent its severity using only four sensor measurements. This method saves huge costs in terms of having advanced equipments such as Laser Vibrometry, instrumentation etc., and yet predict very small damages in large structures; where in traditionally such equipments are necessary.

The paper is organized as follows. First the concept of Wavelet transform is introduced followed by the formulation of Wavelet spectral plate element. Wavelet spectral element also enables measurement of responses at the intermediate location; which are required in the present analysis, through post processing of the nodal solution. Next, the formulation of frequency domain damage index is given. Here, the computation of strain energies in damaged and healthy structure is outlined in detail. The formulated damage measure is then validated through a series of experimental results. The results are performed on two different specimens of different crack orientation and size to ascertain the efficiency of the proposed damaged measure for not only locating the crack but also determining its extent. Next, a compressor blade example is presented, which demonstrates the ability of FDI in predicting very small size damages; wherein the damage location is not known. The paper ends with a brief discussion.

## 2 Wavelet Based Spectral Finite Element (WSFE) Formulation for plates

Here, a complete procedure of reducing the governing partial differential equations of plate to decoupled ODEs using Wavelet transforms in time and space are presented. At the end of the section, response equation in general wave form is derived which is used in the proposed damage measure.

### *2.1 Daubechies Compactly Supported Wavelets*

The details on orthogonal basis of Daubechies wavelets [Daubechis (1992)] is discussed. These wavelets will be used to formulate a spectral plate element required to use base line responses for the structural health monitoring studies. Wavelets, $\psi_{j,k}(t)$ forms compactly supported orthonormal basis for $\mathbf{L^2}(\mathbf{R})$. The wavelets and associated scaling functions $\varphi_{j,k}(t)$ are obtained by translation and dilation of single functions $\psi(t)$ and $\varphi(t)$ respectively.

$$\psi_{j,k}(t) = 2^{j/2}\psi(2^j t - k), \qquad j,k \in \mathbf{Z} \tag{1}$$

$$\varphi_{j,k}(t) = 2^{j/2}\varphi(2^j t - k), \qquad j,k \in \mathbf{Z} \tag{2}$$

Let $P_j(f(t))$ be approximation of a function $f(t)$ in $\mathbf{L^2}(\mathbf{R})$ using $\varphi_{j,k}(t)$ as basis, at

a certain level (resolution) $j$, then

$$P_j(f(t)) = \sum_k c_{j,k}\varphi_{j,k}(t), \qquad k \in \mathbf{Z} \tag{3}$$

where, $c_{j,k}$ are the approximation coefficients. Let $Q_j(f(t))$ be the approximation of the function using $\psi_{j,k}(t)$ as basis, at the same level $j$.

$$Q_j(f(t)) = \sum_k d_{j,k}\psi_{j,k}(t), \qquad k \in \mathbf{Z} \tag{4}$$

where, $d_{j,k}$ are the detail coefficients. The approximation $P_{j+1}(f(t))$ to the next finer level of resolution $j+1$ is given by

$$P_{j+1}(f(t)) = P_j(f(t)) + Q_j(f(t)) \tag{5}$$

This forms the basis of multi resolution analysis associated with wavelet approximation, more details can be found in Reference [Daubechis (1992)].

### *2.2 Governing differential equation for plate*

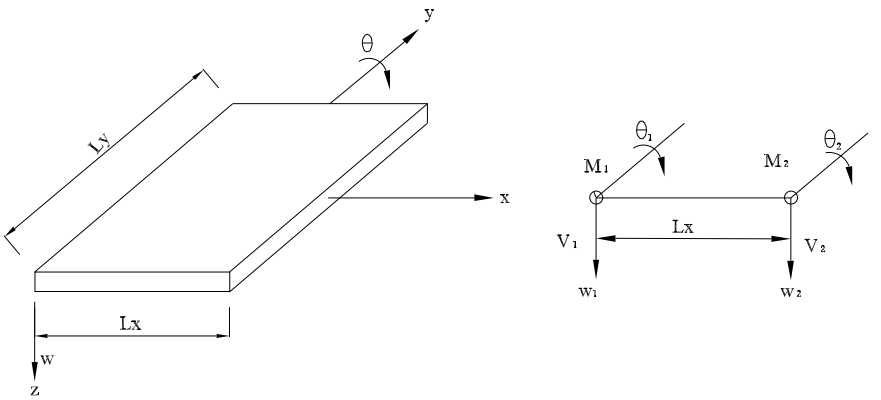


Figure 1: (a) Plate element (b) Nodal forces and displacements

The governing plate equation using Classical Plate Theory [Nayeh and Pai (2004)] for an isotropic material is given by

$$D\left(\frac{\partial^4 w}{\partial x^4} + 2\frac{\partial^4 w}{\partial x^2 \partial y^2} + \frac{\partial^4 w}{\partial y^4}\right) = \rho h \frac{\partial w^2}{\partial t^2} \tag{6}$$

where $D = \frac{Eh}{12(1-\nu^2)}$, E is the modulus of elasticity, $\rho$ is the density, $h$ is the plate thickness and $\nu$ is the Poisson's ratio. $w(x,y,t)$ is the transverse displacement of

plate in the $z$ direction as shown in Fig. 1. The force boundary conditions associated with the governing differential equations are

$$M = D\left(\frac{\partial^2 w}{\partial x^2} + \nu\frac{\partial^2 w}{\partial y^2}\right) \tag{7}$$

$$V = -D\left(\frac{\partial^3 w}{\partial x^3} + (2-\nu)\frac{\partial^3 w}{\partial x \partial y^2}\right) + I_2\frac{\partial \ddot{w}}{\partial x} \tag{8}$$

where, $M$ is the moment, $V$ is the shear force and $I_2$ is the inertial coefficient and is given by

$$I_2 = \int_A \rho z^2 dA \tag{9}$$

### *2.3 Reduction of Wave Equations to ODEs - Temporal Approximation*

The first step of formulation of 2-D WSFE is the reduction of the governing PDEs to another set of PDEs by Daubechies scaling function based transformation in time. The variables are discretized at $n$ points in the time window $[0\ t_f]$. Let $\tau = 0,\ 1, \ldots, n-1$ be the sampling points, then

$$t = (\triangle t)\tau \tag{10}$$

where, $\triangle t$ is the time interval between two sampling points. For example, $w(x,y,t)$, the out of plane transverse displacement of plate, can be approximated by scaling function $\varphi(\tau)$ at an arbitrary scale as

$$w(x,y,t) = w(x,y,\tau) = \sum_k w_k(x,y)\varphi(\tau - k), \quad k \in \mathbf{Z} \tag{11}$$

where, $w_k(x,y)$ (referred as $w_k$ hereafter) are the approximation coefficient at a certain spatial dimension $x$ and $y$. Using these approximations, Eqn. (6) can be written as

$$\sum_k \left(\frac{\partial^4 w_k}{\partial x^4} + 2\frac{\partial^4 w_k}{\partial x^2 \partial y^2} + \frac{\partial^4 w_k}{\partial y^4}\right)\varphi(\tau - k) = \frac{\rho h}{D\triangle t^2}\sum_k w_k \varphi''(\tau - k) \tag{12}$$

Taking inner product on both sides of Eqn. (12) with the translates of scaling functions $\varphi(\tau - j)$, where $j = 0,\ 1, \ldots, n-1$ and using their orthogonal properties, we get $n$ simultaneous PDEs as,

$$\frac{\partial^4 w_j}{\partial x^4} + 2\frac{\partial^4 w_j}{\partial x^2 \partial y^2} + \frac{\partial^4 w_j}{\partial y^4} = \frac{\rho h}{D\triangle t^2}\sum_{k=j-N+2}^{j+N-2} \Omega_{j-k}^2 w_k \quad j = 0,\ 1, \ldots, n-1 \tag{13}$$

where, $N$ is the order of the Daubechies wavelet and $\Omega^2_{j-k}$ are the connection coefficients defined as

$$\Omega^2_{j-k} = \int \varphi''(\tau - k)\varphi(\tau - j)d\tau \tag{14}$$

Similarly, for first order derivative $\Omega^1_{j-k}$ are defined as

$$\Omega^1_{j-k} = \int \varphi'(\tau - k)\varphi(\tau - j)d\tau \tag{15}$$

For compactly supported wavelets, $\Omega^1_{j-k}$, $\Omega^2_{j-k}$ are nonzero only in the interval $k = j-N+2$ to $k = j+N-2$. The details for evaluation of connection coefficients for different orders of derivative is given in reference [Beylkin 1992)]. The Eqn. (13) are converted to to a set of coupled PDEs given as

$$\left\{\frac{\partial^4 w_j}{\partial x^4}\right\} + 2\left\{\frac{\partial^4 w_j}{\partial x^2 \partial y^2}\right\} + \left\{\frac{\partial^4 w_j}{\partial y^4}\right\} = \frac{\rho h}{D}[\Gamma^1]^2\{w_j\} \tag{16}$$

where $\Gamma^1$ is the first order connection coefficient matrix obtained after using the wavelet extrapolation technique [Williams and Amaratunga (1997)]. It should be mentioned here that though the connection coefficients matrix, $\Gamma^2$, for second order derivative can be obtained independently, here it is written as $[\Gamma^1]^2$ as it helps to impose the initial conditions [Mitra and Goplakrishnan (2005)]. These coupled PDEs are decoupled using eigenvalue analysis

$$\Gamma^1 = \Phi\Pi\Phi^{-1} \tag{17}$$

where, $\Pi$ is the diagonal eigenvalue matrix and $\Phi$ is the eigenvectors matrix of $\Gamma^1$. The eigenvalues be denoted as $\imath\gamma_j$, where $\imath = \sqrt{-1}$, using these, the decoupled ODEs corresponding to Eqn. 16 is given by

$$\frac{\partial^4 \widehat{w}_j}{\partial x^4} + 2\frac{\partial^4 \widehat{w}_j}{\partial x^2 \partial y^2} + \frac{\partial^4 \widehat{w}_j}{\partial y^4} = -\frac{\rho h}{D}\gamma_j^2 \widehat{w}_j \quad j = 0,\ 1, \ldots, n-1 \tag{18}$$

where, $\widehat{w}_j$ is the transformed displacement and is given by

$$\widehat{w}_j = \Phi^{-1} w_j \tag{19}$$

### *2.4 Reduction of Wave Equations to ODEs - Spatial Approximation*

The next step involved is to further reduce each of the transformed and decoupled PDEs given by Eqn. (18) for $j = 0,\ 1, \ldots, n-1$ to a set of coupled ODEs using Daubechies scaling function approximation in $(Y)$ direction. Similar to time

approximation, the transformed variable $\widehat{w}_j$ be discretized at $m$ points in the spatial window $[0\ L_Y]$, where $L_Y$ is the length in $Y$ direction (see Fig. 1). Let $\zeta = 0,\ 1,\ldots,\ m-1$ be the sampling points, then

$$y = \triangle Y \zeta \tag{20}$$

where, $\triangle Y$ is the spatial interval between two sampling points. The function $\widehat{w}_j(x,y)$ can be approximated by scaling function $\varphi(\zeta)$ at an arbitrary scale as

$$\widehat{w}_j(x,y) = \widehat{w}_j(x,\zeta) = \sum_k \widehat{w}_{lj}(x)\varphi(\zeta - l), \qquad l \in \mathbf{Z} \tag{21}$$

where, $\widehat{w}_{lj}(x,y)$ (referred as $\widehat{w}_{lj}$ hereafter) are the approximation coefficient at a certain spatial dimension $x$. Therefore, the Eqn. (18) can be written as

$$\sum_l \frac{d^4\widehat{w}_{lj}}{dx^4}\varphi(\zeta - l) + \frac{2}{\triangle Y^2}\sum_l \frac{d^2\widehat{w}_{lj}}{dx^2}\varphi''(\zeta - l) + \frac{1}{\triangle Y^4}\sum_l \widehat{w}_{lj}\varphi''''(\zeta - l) = -\frac{\rho h}{D}\gamma_j^2 \sum_l \widehat{w}_{lj}\varphi(\zeta - l) \tag{22}$$

Taking inner product on both sides of Eqn. (22) with the translates of scaling functions $\varphi(\zeta - i)$, where $i = 0,\ 1,\ldots,m-1$ and using their orthogonal properties, we get $m$ simultaneous ODEs as,

$$\frac{d^4\widehat{w}_{ij}}{dx^4} + \frac{2}{\triangle Y^2}\sum_{l=i-N+2}^{i+N-2} \frac{d^2\widehat{w}_{ij}}{dx^2}\Omega_{i-l}^2 + \frac{1}{\triangle Y^4}\sum_{l=i-N+2}^{i+N-2} \widehat{w}_{ij}\Omega_{i-l}^4 = -\frac{\rho h}{D}\gamma_j^2\widehat{w}_{ij} \quad i = 0,\ 1,\ldots,m-1 \tag{23}$$

where, $N$ is the order of Daubechies wavelet, $\Omega_{i-l}^1$ and $\Omega_{i-l}^2$ are the connection coefficients for first and second order derivative defined in Eqns. (15) and (14) respectively. The unknown coefficients lying outside the finite domain in terms of the inner coefficients are obtained using periodic extension or restrain matrix [Patton and Marks (1996)]. Considering the periodic extension, the ODEs given by Eqn. (23) can be written as a matrix equation of the form

$$\left\{\frac{d^4 w_{ij}}{dx^4}\right\} + 2[\Lambda^1]^2\left\{\frac{d^2 w_{ij}}{dx^2}\right\} + [\Lambda^1]^4\left\{\widehat{w}_{ij}\right\} = -\frac{\rho h}{D}\gamma_j^2\left\{\widehat{w}_{ij}\right\} \tag{24}$$

where, $[\Lambda^1]$ is the first order connection coefficient matrix obtained after periodic extension and it is of the form

$$[\Lambda^1] = \frac{1}{\triangle Y}\begin{bmatrix} \Omega_0^1 & \Omega_{-1}^1 & \dots & \Omega_{-N+2}^1 & \dots & \Omega_{N-2}^1 \dots \Omega_1^1 \\ \Omega_1^1 & \Omega_0^1 & \dots & \Omega_{-N+3}^1 & \dots & 0 \dots \Omega_2^1 \\ \vdots & \vdots & \dots & \vdots & \dots & \vdots \dots \vdots \\ \Omega_{-1}^1 & \Omega_{-2}^1 & \dots & 0 & \dots & \Omega_{N-3}^1 \dots \Omega_0^1 \end{bmatrix} \tag{25}$$

It should be mentioned here that though the connection coefficient matrices of higher order derivatives can be obtained independently, here it is written for second order derivative as $[\Lambda^2] = [\Lambda^1]^2$ and fourth order derivative as $[\Lambda^4] = [\Lambda^1]^4$ as it helps to impose initial conditions. The coupled ODEs given in Eqn. (24) are decoupled using eigenvalue analysis similar to that done in time approximation as

$$\Lambda^1 = \Psi \Upsilon \Psi^{-1} \tag{26}$$

where, $\Upsilon$ is the diagonal eigenvalue matrix and $\Psi$ is the eigenvectors matrix of $\Lambda^1$. It should be mentioned here that matrix $\Lambda^1$ has a circulant form and its eigen parameters are known analytically [Davis (1963)]. The eigenvalues are denoted as $\imath\beta_i$, using these, the decoupled ODE's corresponds to Eqn. (24) is given by

$$\frac{d^4\widetilde{w}_{ij}}{dx^4} - 2\beta_i^2\frac{d^2\widetilde{w}_{ij}}{dx^2} + \beta_i^4\widetilde{w}_{ij} = -\frac{\rho h}{D}\gamma_j^2\widetilde{w}_{ij} \;\; i = 0,\ 1, \dots, m-1 \tag{27}$$

where, $\widetilde{w}_{ij}$ is the transformed displacement and is given by

$$\widetilde{w}_{ij} = \Psi^{-1}\widehat{w}_{ij} \tag{28}$$

Similarly, the transformed form of the force boundary conditions given in Eqns. (7) and (8) are given by

$$D\left(\frac{d^2\widetilde{w}_{ij}}{dx^2} - \beta_i^2\nu\widetilde{w}_{ij}\right) = \widetilde{M}_{ij} \tag{29}$$

$$-D\left(\frac{d^3\widetilde{w}_{ij}}{dx^3} + \beta_i^2(2-\nu)\frac{d\widetilde{w}_{ij}}{dx}\right) - I_2\gamma_j^2\frac{d\widetilde{w}_{ij}}{dx} = \widetilde{V}_{ij}, \;\; i = 0, 1, \dots, m-1 \tag{30}$$

The final transformed ODEs given by Eqn. (27), the boundary conditions Eqns. (29) and (30) are used in 2-D WSFE [Mitra and Goplakrishnan (2006)], following a procedure very similar to 2-D FSFE formulation [Chakraborty and Gopalakrishnan (2004), (2005)] and is explained in the next subsection.

### 2.5 Spectral Finite Element Formulation

Here, spectral finite element formulation for plate element with associated degree of freedom is discussed. Procedure is outlined for obtaining the solution of Eqn. (27) along with wave numbers in x and y direction.

The degrees of freedom associated with the element formulation is shown in Fig. 1(b). The element has two degrees of freedom per node, which are $\widetilde{w}_{ij}$ and $\partial\widetilde{w}_{ij}/\partial x$. From the previous sections, for unrestrained lateral edges we get a set of decoupled ODEs Eqn. (27) for isotopic plate using CPT, in a transformed wavelet domain. These equations are required to be solved for $\widetilde{w}_{ij}$ and the actual solutions $w(x,y,t)$ are obtained using inverse wavelet transform twice for spatial $(Y)$ dimension and time $(t)$. For finite length data, the wavelet transform and its inverse can be obtained using a transformation matrix [Williams and Amaratunga (1994)].

It can be seen that the transformed decoupled ODEs have a form similar to that in FSFE [Doyle (1999)] and thus, WSFE can be formulated following the same method as for FSFE formulation. In this section, the subscripts $j$ and $i$ are dropped hereafter for simplified notations and all the following equations are valid for $j = 0,\ 1,\ \ldots,\ n-1$ and $i = 0,\ 1,\ \ldots,\ m-1$ for each $j$. Let, the solution of the Eqn. (27) be of the form,

$$\widetilde{w} = \sum_{r=1}^{4} a_r e^{-ik_r x} \tag{31}$$

where, $k_r$ are wave numbers and $a_r$ are the wave amplitudes. The exact interpolating functions for an element of length $L_X$ is obtained by substituting Eqn. (31) in Eqn. (27), which can be derived in matrix form

$$\{\widetilde{w}(x)\}^T = [\mathbf{R}][\Theta]\{\mathbf{a}\} \tag{32}$$

where, $[\Theta]$ is a diagonal matrix with the diagonal terms $[e^{-k_1 x},\ e^{-k_1(L_X-x)},\ e^{-k_2 x},\ e^{-k_2(L_X-x)}]$ and $[\mathbf{R}] = [R_{11}\ \ R_{12}\ \ R_{13}\ \ R_{14}]$ is a $1\times 4$ amplitude ratio matrix for each set of $k_1$ and $k_2$, where $k_1$ and $k_2$ are wave numbers of the transverse and rotational modes. These $k_1$ and $k_2$ are obtained by substituting Eqn. (31) in Eqn. (27) and solving the characteristic equation. The characteristic equation is obtained by equating the determinant of the $1\times 1$ companion matrix to zero and is as follows. Substituting the assumed solution (Eqn. 31) in the set of ODEs (Eqn. 27), a PEP is posed as to find $(\mathbf{v},k)$, such that

$$\psi(k)\mathbf{v} = (k^4\mathbf{A}_4 + k^2\mathbf{A}_2 + \mathbf{A}_0)\mathbf{v} = 0\ , \quad \mathbf{v}\neq 0 \tag{33}$$

where $k$ is an eigenvalue and $\mathbf{v}$ is the corresponding eigenvector.

$$\mathbf{A}_4 = 1$$
$$\mathbf{A}_2 = 2\beta_i^2$$
$$\mathbf{A}_0 = \beta_i^4 + \frac{\rho h \gamma_j^2}{D}$$

The PEP is solved, the spectrum relation is quartic polynomial of $m = k$,

$$p(m) = m^4 + C_2 m^2 + C_4 \tag{34}$$

which generates a companion matrix of order 1.

The corresponding $[\mathbf{R}]$ is obtained using singular value decomposition of the matrix. This method of determining wave numbers and corresponding amplitude ratios was developed to formulate FSFE for graded beam with Poisson's contraction [Chakraborty and Gopalakrishnan (2004)], $k_1$ and $k_2$ corresponds to the two modes i.e transverse and rotational. As explained in reference [Mitra and Goplakrishnan (2006)], these are the wave numbers but only up to a certain fraction of Nyquist frequency.

Here, $\{\mathbf{a}\} = \{\text{A, B, C, D}\}$ are the unknown wave coefficients to be determined from transformed nodal displacements $\{\widetilde{\mathbf{u}}^{\mathbf{e}}\}$, where $\{\widetilde{\mathbf{u}}^{\mathbf{e}}\} = \{\widetilde{w}_1 \ \partial\widetilde{w}_1/\partial x \ \widetilde{w}_2 \ \partial\widetilde{w}_2/\partial x\}$ and $\widetilde{w}_1 \equiv \widetilde{w}(0)$, $\partial\widetilde{w}_1/\partial x \equiv \partial\widetilde{w}(0)/\partial x$ and $\widetilde{w}_2 \equiv \widetilde{w}(L_X)$, $\partial\widetilde{w}_2/\partial x \equiv \partial\widetilde{w}/\partial x(L_X)$, (see Fig. 1(b) for the details of degree of freedom that the element can support). Thus, we can relate the nodal displacements and unknown coefficients as

$$\{\widetilde{\mathbf{u}}^{\mathbf{e}}\} = [\mathbf{B}]\{\mathbf{a}\} \tag{35}$$

From the forced boundary conditions, Eqns. (29) and (30), nodal forces and unknown coefficients can be related as

$$\{\widetilde{\mathbf{F}}^{\mathbf{e}}\} = [\mathbf{C}]\{\mathbf{a}\} \tag{36}$$

where, $\{\widetilde{\mathbf{F}}^{\mathbf{e}}\} = \{\widetilde{V}_1 \ \widetilde{M}_1 \ \widetilde{V}_2 \ \widetilde{M}_2\}$ and $\widetilde{V}_1 \equiv -\widetilde{V}(0)$, $\widetilde{M}_1 \equiv -\widetilde{M}(0)$ and $\widetilde{V}_2 \equiv \widetilde{V}(L_X)$, $\widetilde{M}_2 \equiv \widetilde{M}(L_X)$ (see Fig. 1(b)). From Eqns. 35 and 36 we can obtain a relation between transformed nodal forces and displacements similar to conventional FE

$$\{\widetilde{\mathbf{F}}^{\mathbf{e}}\} = [\mathbf{C}][\mathbf{B}]^{-1}\{\widetilde{\mathbf{u}}^{\mathbf{e}}\} = [\widetilde{\mathbf{K}}^{\mathbf{e}}]\{\widetilde{\mathbf{u}}^{\mathbf{e}}\} \tag{37}$$

where $[\widetilde{\mathbf{K}}^{\mathbf{e}}]$ is the exact elemental dynamic stiffness matrix. After the constants $\{\mathbf{a}\}$ are known from the above equations, they can substituted back in Eqn. (32) to obtain the transformed displacements $\widetilde{w}$, $\partial\widetilde{w}/\partial x$ at any given $x$.

As said before, $k_1$ and $k_2$ are wave numbers in $x$ direction are obtained by solving the Eqn. (27). The wave numbers in $y$ direction are given as $\beta$ from Eqn. (26). Therefore, the transformed displacement $\tilde{w}(x,y)$ can be written as,

$$\tilde{w}(x,y) = [Ae^{-ik_1x} + Be^{-ik_1(L-x)} + Ce^{-ik_2x} + De^{-ik_2(L-x)}]e^{i\beta y} \tag{38}$$

Here $\{A,\ B,\ C,\ D\}$ are the wave coefficients to be determined either by the boundary conditions or the four wave based measurements. The later method is used for developing the new damage measure, which is discussed in the next section.

## 3 Formulation of New damage measure based on frequency domain Energy

In this section, a brief description on grid generation is discussed followed by energy calculations and damage index are derived. Next, the experimental set up and the proposed damage index using four measurements is presented. The entire analysis is performed in frequency domain. The damage measure is defined in the frequency domain as the ratio of energy parameter in healthy structure to the damaged structure.

### *3.1 Grid generation*

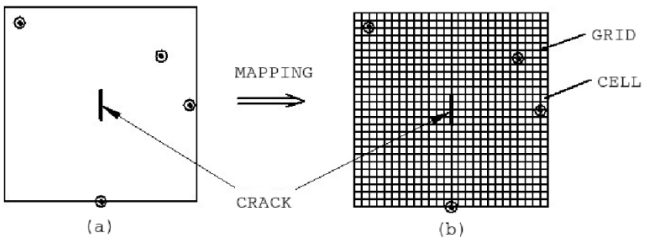


Figure 2: (a) Damage specimen used in experiment; (b) Grid generation of the same specimen used in simulation.

The mesh generation of the structure used in the formulation of a new damage measure is given below. Fig. 2(a) represents the actual (damaged) specimen with a $90^0$ crack used in conducting the experiments and Fig. 2(b) indicates the grid generated on this specimen to be used in the numerical simulation. The given geometry is divided into number of uniform spaced cells with cell size as 2-6mm in x and y directions. Each cell is treated as an element and the grid as node. The

experimental response (signal) is captured at any four points of the plate as shown in Fig. 2(a). These obtained signals are mapped on to the four corresponding location grid points (nodes) of the discretized structure as in Fig. 2(b) and are used in the rest of the simulation. Similar steps are adopted for the healthy and other damaged structures too.

### *3.2 Computation of undamaged Strain energy*

In the entire simulation of this paper, it is assumed that the wave numbers do not change with the presence of small size cracks i.e. the wave numbers are the same for healthy and damaged structure, which are computed as per Eqn. (27) for a healthy structure. The formulated wavelet spectral plate element as in Section. 2 is used to compute the responses at all the grid points (nodes). The response is interpolated at all intermediate grid locations using the new formulation and is described in the last subsection.

The response at any locations $(x,y)$ on undamaged structure can be written in general wave form as

$$\tilde{w}^*(x,y) = [Ae^{-ik_1x} + Be^{-ik_1(L-x)} + Ce^{-ik_2x} + De^{-ik_2(L-x)}]e^{i\beta y} \tag{39}$$

Here, the four wave coefficients $A,B,C,D$ are obtained from measurements at any four points on undamaged structure. The experimental setup is discussed in the next sub section and choice of these four points are outlined in the next section. Using these responses, the corresponding strain and stress calculated and are given by,

$$\begin{aligned}
\varepsilon^*{}_{xx} &= \partial\tilde{w}^*/\partial x \\
&= [-ik_1Ae^{-ik_1x} + ik_1Be^{-ik_1(L-x)} - ik_2Ce^{-ik_2x} + ik_2De^{-ik_2(L-x)}]e^{i\beta y} \qquad (40)\\
\sigma^*{}_{xx} &= E\varepsilon^*{}_{xx} \\
&= E[-ik_1Ae^{-ik_1x} + ik_1Be^{-ik_1(L-x)} - ik_2Ce^{-ik_2x} + ik_2De^{-ik_2(L-x)}]e^{i\beta y} \qquad (41)
\end{aligned}$$

The energy parameter in frequency domain is evaluated by integrating the strain energy over the cell domain using these stresses and strains. This process is repeated for all the cells. For the healthy structure, the energy parameter at the $i^{th}$ element is given by $\hat{U}_i^*$

$$\hat{U}_i^* = \frac{1}{2}\int_V (\sigma^*{}_{xx}\varepsilon^*{}_{xx} + \sigma^*{}_{yy}\varepsilon^*{}_{yy} + \tau^*{}_{xy}\gamma^*{}_{xy})dV^* \tag{42}$$

where $dV^* = dxdyh$. Here $dx$ and $dy$ are the grid sizes in x and y direction respectively, h is the thickness of the plate.

### 3.3 Computation of damaged Strain energy

Here, it is considered the the size of the damaged plate is same as that of the undamaged plate but with cracks at the center of the plate. The response at any locations $(x,y)$ on the damaged plate can be written in general wave form as

$$\tilde{w}(x,y) = [A_1 e^{-ik_1 x} + B_1 e^{-ik_1(L-x)} + C_1 e^{-ik_2 x} + D_1 e^{-ik_2(L-x)}]e^{i\beta y} \tag{43}$$

Here, the four wave coefficients $A_1, B_1, C_1, D_1$ are obtained from measurements at any four points on damaged structure. The choice of these four points are outlined in the next section. The corresponding strain and stress are calculated using the responses obtained from the damaged plate and are given by,

$$\begin{aligned}\varepsilon_{xx} =& \partial\tilde{w}/\partial x \\ =& [-ik_1 A_1 e^{-ik_1 x} + ik_1 B_1 e^{-ik_1(L-x)} - ik_2 C_1 e^{-ik_2 x} + ik_2 D_1 e^{-ik_2(L-x)}]e^{i\beta y} \qquad (44)\\ \sigma_{xx} =& E\varepsilon_{xx} \\ =& E[-ik_1 A_1 e^{-ik_1 x} + ik_1 B_1 e^{-ik_1(L-x)} - ik_2 C_1 e^{-ik_2 x} + ik_2 D_1 e^{-ik_2(L-x)}]e^{i\beta y} \qquad (45)\end{aligned}$$

The energy parameter in frequency domain is evaluated by integrating the strain energy over the cell domain using these stresses and strains. This process is repeated for all the cells. For the damaged structure, the energy parameter at the $i^{th}$ element is given by $\hat{U}_i$

$$\hat{U}_i = \frac{1}{2}\int_V (\sigma_{xx}\varepsilon_{xx} + \sigma_{yy}\varepsilon_{yy} + \tau_{xy}\gamma_{xy})dV \tag{46}$$

where $dV = dxdyh$. Here $dx$ and $dy$ are the grid sizes in x and y direction respectively, h is the thickness of the plate.

### 3.4 Frequency domain Damage Index

The energies calculated as above are used to find the damage index. The frequency domain damage index (FDI) is defined as the ratio of the energies of the undamaged to the damaged structures and is given by

$$\hat{\mathrm{d}}_{\mathrm{i}}(\omega_{\mathrm{n}}) = \frac{\hat{\mathrm{U}}_{\mathrm{i}}^{*}}{\hat{\mathrm{U}}_{\mathrm{i}}} \tag{47}$$

Damage index at $i^{th}$ element over all frequencies up to Nyquist frequency i.e. $\frac{N}{2}$ is

$$D_i = \sum_{\omega_n} |\hat{d}_i|, \qquad i \in [1,m], \qquad n = 1...\frac{N}{2} \tag{48}$$

Note that, the inertial component is built into the formulation due to the usage of Spectral FEM. The baseline energy is again obtained by spectral FEM analysis of healthy specimen. This does not add to computational cost due to small size of spectral stiffness which is $4 \times 4$. Here, a new approach is demonstrated to get Damage Index through only four measurements. In the next section, it is demonstrated on a square Aluminum plate of different crack orientation and on compressor blade made of titanium in which the crack is very small.

### *3.5 Experimental setup*

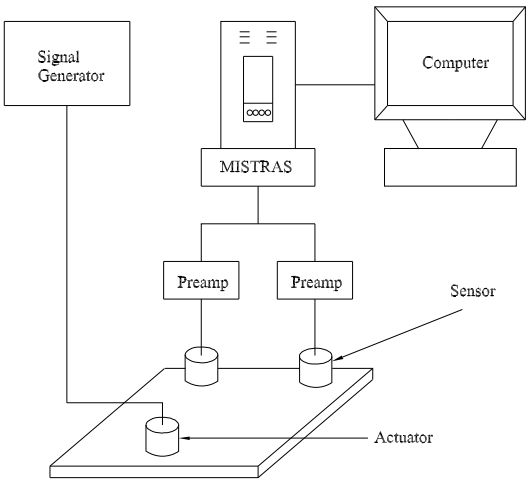


Figure 3: Block diagram of Experimental setup.

The block diagram of the experimental setup and the photograph of the experimentation is shown in Fig. 3 and Fig. 4 respectively. The PZT sensors are mounted on the Aluminum specimen at the locations(1,2,.....8) shown in Fig. 5. One of the sensors will act as an actuator(at location 8) which is connected to the signal generator and remaining sensors will act as signal receivers. Signals are recorded using MISTRAS software. Experiments are conducted on healthy specimen and the damaged specimens with a center crack at 0,45,90 degrees and the signals are recorded and this data is used in numerical simulations.

### *3.6 Damage Index through only four measurements*

In this case a square plate of size $\times 0.13m \times 0.13m \times 0.004m$ (healthy specimen) shown in Fig. 5(a) is considered. At points 1,3,5 and 7 accelerometers are placed

Figure 4: Photograph of the setup.

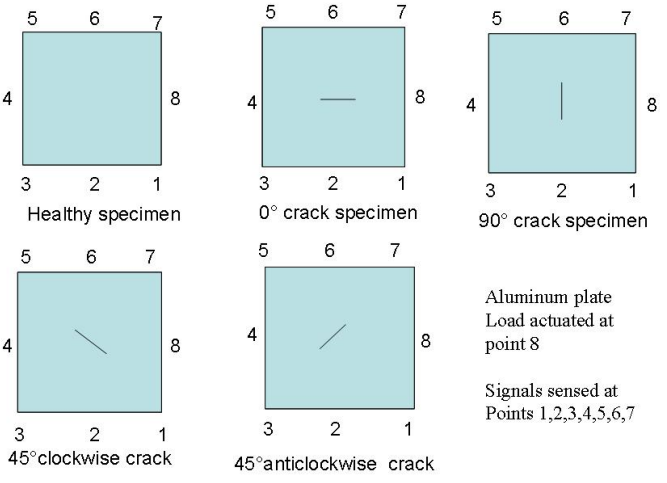


Figure 5: Aluminum specimens with different crack orientation

and subjected to a random tone burst signal at point 8. Similar experiments are performed on same size plates with the same crack size (20mm) but with different orientation as shown in Figs. 5(b), (c), (d) and (e), respectively. The signals are recorded from healthy and damage specimens at these four locations. These signals are used in the numerical simulation as below. The general wave form in frequency domain at any point is given by Eqn. (38). The signals recorded at any

four locations $(x,y)$ can be written in general wave form as

$$\tilde{w}_1(x_1,y_1) = [Ae^{-ik_1x_1} + Be^{-ik_1(L-x_1)} + Ce^{-ik_2x_1} + De^{-ik_2(L-x_1)}]e^{i\beta y_1}$$
$$\tilde{w}_2(x_2,y_2) = [Ae^{-ik_1x_2} + Be^{-ik_1(L-x_2)} + Ce^{-ik_2x_2} + De^{-ik_2(L-x_2)}]e^{i\beta y_2}$$
$$\tilde{w}_3(x_3,y_3) = [Ae^{-ik_1x_3} + Be^{-ik_1(L-x_3)} + Ce^{-ik_2x_3} + De^{-ik_2(L-x_3)}]e^{i\beta y_3}$$
$$\tilde{w}_4(x_4,y_4) = [Ae^{-ik_1x_4} + Be^{-ik_1(L-x_4)} + Ce^{-ik_2x_4} + De^{-ik_2(L-x_4)}]e^{i\beta y_4}$$

where, the wave numbers $k_1$, $k_2$ in $x$ and $\beta$ in $y$ direction and are computed as Eqns. (27) and (26) and will depend only on frequency. As mentioned earlier, these wave numbers are assumed to be the same for damaged and healthy specimens when the damage sizes are very small.

The above equations can be written in more compact form $\{\mathbf{W}\} = [\mathbf{M}]\{\mathbf{C}\}$. Here $\{\mathbf{W}\}$ and $\{\mathbf{C}\}$ are $4 \times 1$ vectors, $[\mathbf{M}]$ is a matrix of size $4 \times 4$. Therefore, the above matrix form can be written as $\{\mathbf{C}\} = [\mathbf{M}]^{-1}\{\mathbf{W}\}$, using this the unknown vector i.e. wave coefficients, $\{\mathbf{C}\} = \{A\ B\ C\ D\}^T$ is evaluated, as all other parameters are known. Once, the wave coefficients at each frequency $(\omega)$ are known, the wave form at any location $(x,y)$ is obtained by Eqn.( 39) on healthy specimen and Eqn.( 43) on damaged specimen. The corresponding strain, stress, energy parameter in healthy and damaged structure are evaluated using the Eqns. (40-42) and Eqns. (44-46) respectively . The derived frequency domain damage index (Eqn. 48) is used to get the damage measure of different structures and the numerical results are reported in the next section.

## 4 Numerical Results

Here, three different examples are considered to demonstrate the efficiency of the proposed damage index to predict the location and extent of the damage. In the first example, aluminum specimens with different crack orientation (shown in Fig. 5) are considered. All the specimens have the same size of $0.13m \times 0.13m \times 0.004m$ and the length of the crack is 0.20m. These specimens are used to find the effect of signal location on damage index and to generate FDI plots using just four measurements. Next, a plate of different dimension with a small crack oriented at $90^0$ is considered to find FDI. Finally, a turbine blade with a very small crack is used to demonstrate this technique to predict the damage location.

### *4.1 Selection procedure for the four sensor locations*

The details of the different specimens and sensor location are shown in Fig. 5. First, the plate with $90^\circ$ crack and a healthy plate are considered to study the best

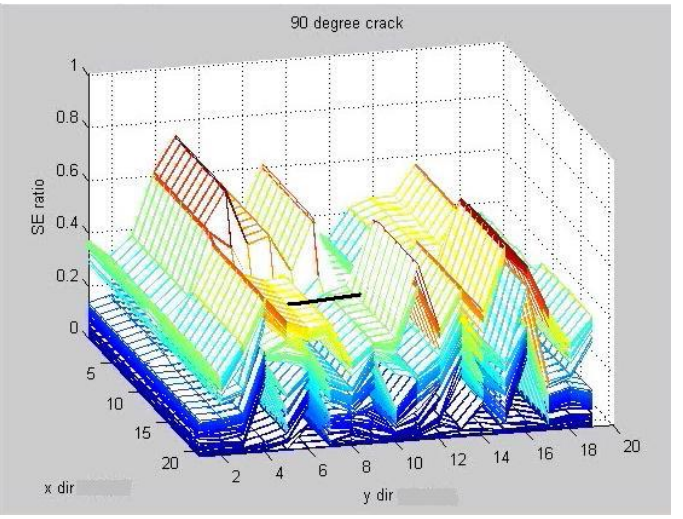


Figure 6: Snapshot of normalized FDI plot with 1-2-4-6 sensor locations on 90° crack specimen.

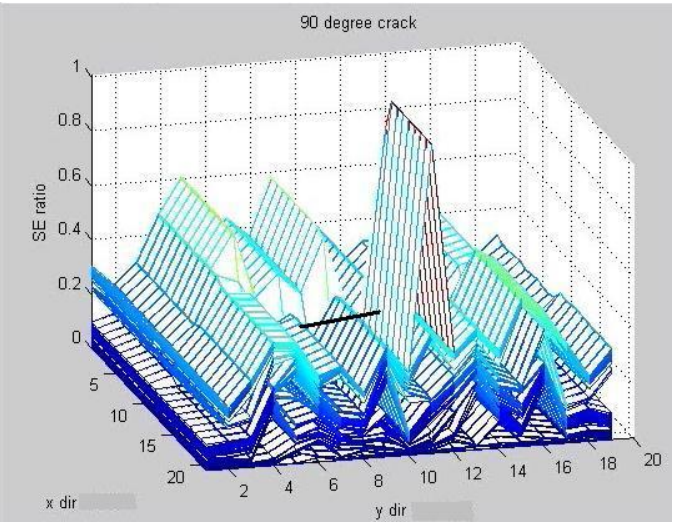


Figure 7: Snapshot of normalized FDI plot with 1-2-5-6 sensor locations on 90° crack specimen.

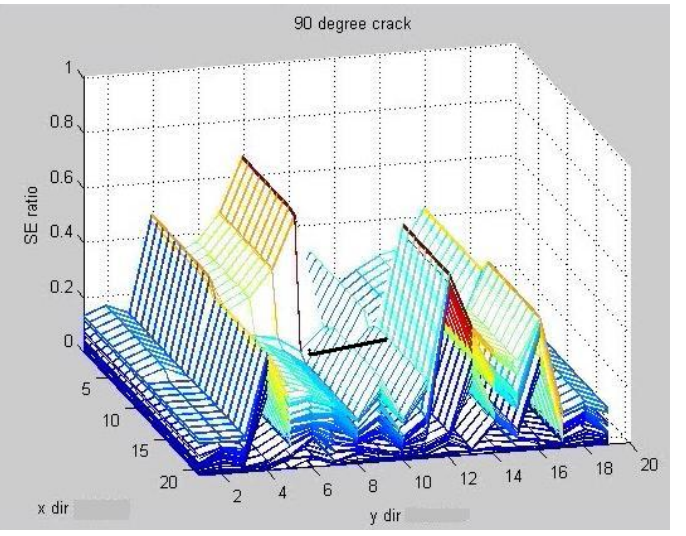


Figure 8: Snapshot of normalized FDI plot with 1-2-6-7 sensor locations on 90° crack specimen.

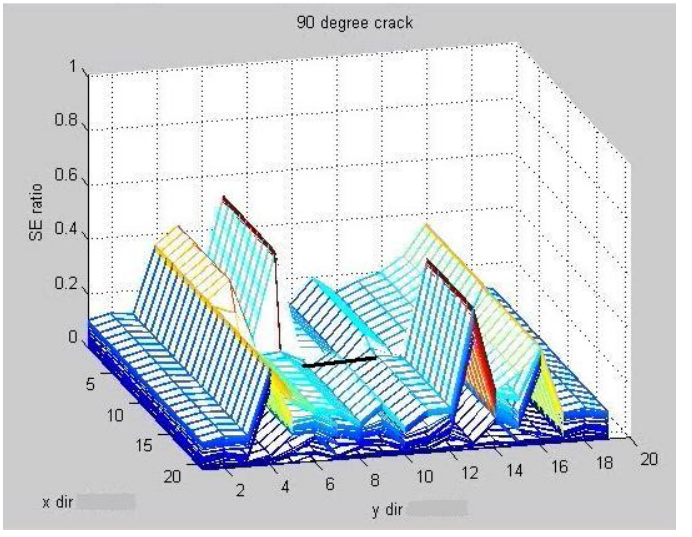


Figure 9: Snapshot of normalized FDI plot with 2-3-5-6 sensor locations on 90° crack specimen.

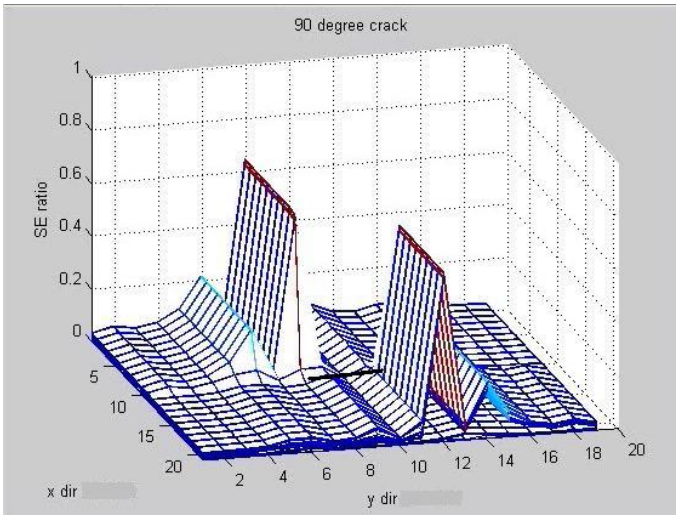


Figure 10: Snapshot of normalized FDI plot with 1-3-5-7 sensor locations on 90° crack specimen.

possible locations for sensor placements. The responses are measured at the sensor locations in five different combinations, namely 1-2-4-6, 1-2-5-6, 1-2-6-7, 2-3-5-6 and 1-3-5-7 respectively and the response information in the exterior of the plate is regenerated for different sensor combination using spectral finite elements. The responses are reconstructed over a square grid spaced at an interval of $4mm$ in both direction. The FDI plots are then generated up to the Nyquist frequency i.e $\frac{N}{2}$. A few snapshots of the FDI, zoomed near the cracks are shown in Fig. 6. Note that in all the following figures, dark black line represents the approximate crack position. From Figs. 6, 7, 8, 9, it indicates that many peaks appear near and surrounding the crack. These scattering may be due to improper collection of data from the sensors. But, from Fig. 10 it is noted that the peaks are concentrated near the crack.

From these observations, it is concluded that, out of all the possible signal recording location arrangements, 1-3-5-7 gives the best indication of crack presence and its location i.e. the peaks represents high energy ratio due to singular stress field and it occurs near the crack, which indicates the presence of the damage. Hence, for effective damage detection, the four sensor points should be located symmetric with respect to crack location. Hence, 1-3-5-7 is the optimum sensor locations which gives the maximum sensitivity and will be used as sensor locations for further examples.

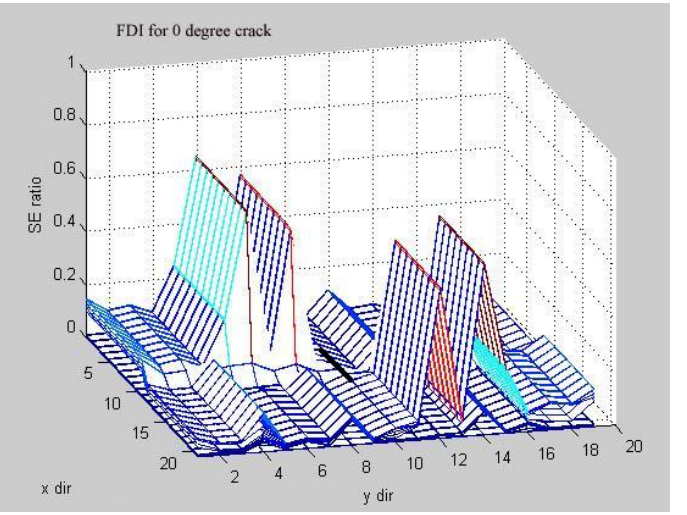


Figure 11: Snapshot of normalized FDI plot for 0° crack orientation.

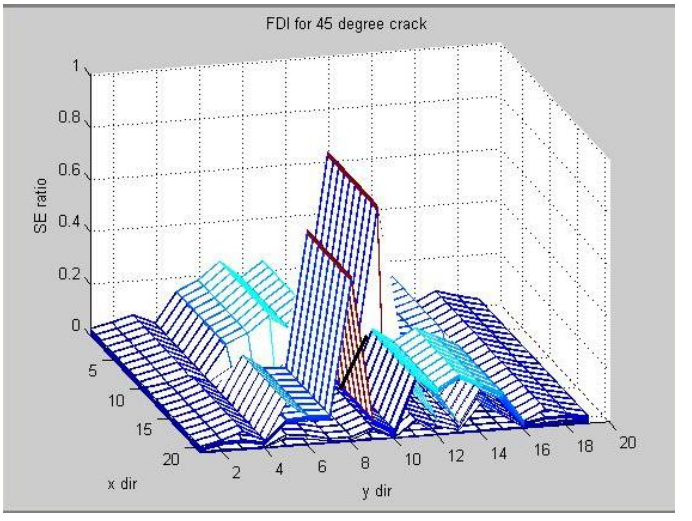


Figure 12: Snapshot of normalized FDI plot for 45° crack orientation.

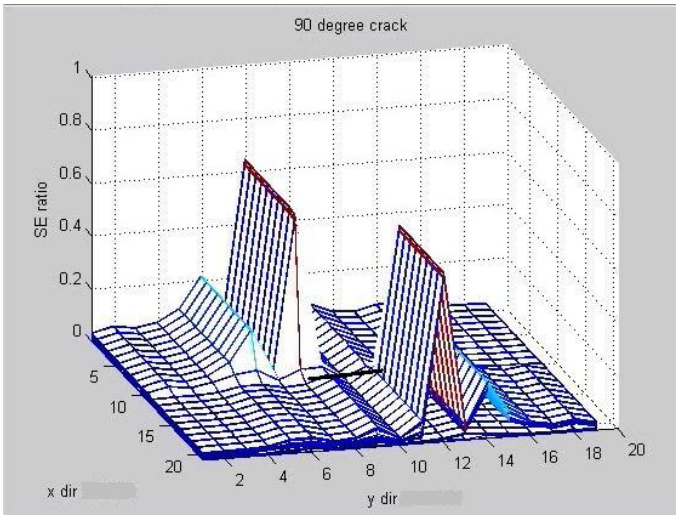


Figure 13: Snapshot of normalized FDI plot for 90° crack orientation.

### *4.2 FDI for different crack orientations*

Here, square aluminum plates with 20mm crack oriented at 0°, 45° and 90° are considered with the sensor location 1-3-5-7. Also, a healthy plate with the same dimension is used. The FDI plots are generated up to the Nyquist frequency i.e $\frac{N}{2}$. Few snapshots of the FDI, near the cracks are shown in Figs. 11, 12, 13. As discussed previously for the $90^0$ case, here also; in all the cases (0°, 45° and 90° cracks) peaks are observed at the two crack tip locations, indicating clearly the presence and extent of cracks. The peak patterns are systematically getting shifted due to the change in orientation of the crack.

### *4.3 FDI for different crack sizes*

In the previous subsection 20mm crack with $90^0$ crack results are presented. To demonstrate the uniqueness of the proposed method, the damage index for different crack sizes are presented. Here, a small through width crack of size $10mm$ introduced exactly at the middle of the plate with $90^0$ orientation and data is captured for computing damage index using the proposed FDI.

A broad band signal of $50\mu sec$ duration is induced in the specimen using a PZT actuator placed at the location 8 of the specimen as shown in Fig. 5. The Fig. 14. shows the FDI plot over the region. From the figure, it is clearly seen that the value of damage index peaks at the two crack tips indicating, not only the location,

but also the extent. The peak pattern looks very similar to that of Fig. 13. which represents the crack zone. This also proves the consistency of the proposed method. FDI enables region-by-region analysis, which results in enormous saving of time in the real-time health monitoring sense.

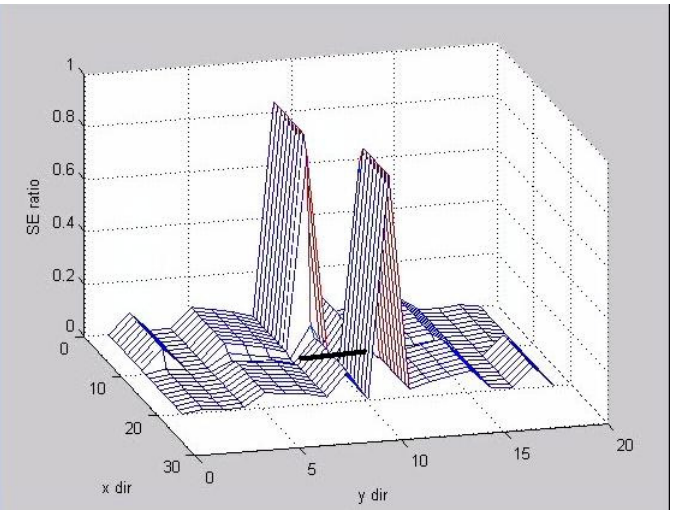


Figure 14: Snapshot of normalized FDI plot for 90° crack orientation.

### *4.4 FDI for Compressor blade*

Next, damage detection using FDI is extended to more practical structures, namely the compressor blade (made from titanium alloy) used in Gas Turbine construction. The important aspect of this example is that the damage is very small.

As before, forcing is introduced through a small PZT disc actuator placed at the mid point of the tip of the blade. Here, a broad band square signal of pulse width $5\mu sec$ is fed into PZT actuator. The signals are sensed at four locations with the area cover up of $30mm \times 60mm$ at the center of blade.

Fig. 15. shows the plot of FDI produced using measured data. The plot clearly shows two large peaks occurring very close to each other indicating the presence of damage. The area marked with a square represents the crack zone. This example clearly demonstrates the ability of FDI in predicting very small size damages.

The main novelty in the paper is that the proposed method can predict very small damages using just four measurements. That is, using these four measurements, the responses at the number of locations in structure can be interpolated. In essence,

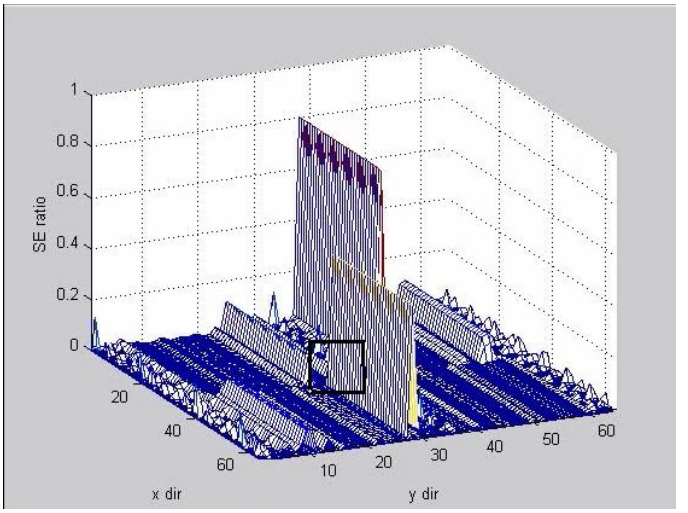


Figure 15: Snapshot of normalized FDI for compressor blade.

the present method can effectively replace the costly equipments such as Scanning Laser Vibrometer normally used in structural health monitoring studies; which can give seamless non contact measurement over a large area. In addition to above, the following are the additional advantages of the method. 1) The method can handle both low and high frequency input signal, which are normally required for determining small damage. 2) The model sizes are very small and hence the damage location, its size and its orientation can be obtained rapidly with in few seconds, unlike conventional methods based on Finite Element modeling.

## 5 Conclusions

This paper presents a novel damage detection scheme based on strain energy defined in the frequency domain. The method extensively uses wavelet spectral finite element for not only obtaining the base line information, but also to reconstruct the responses at many intermediate locations using any four measured responses. The approach was used to predict damages in different specimens having different damage sizes and orientation. It was shown that the approach was able to capture very small damages. When the method is used with only four sensor measurement, the location of sensor with respect to damage plays a very important part on the accuracy of the measurement.

## References

**Beylkin, G.** (1992): On the representation of operators in bases of compactly supported wavelets. *SIAM Journal of Numerical Analysis*, vol. 6, no. 6, pp. 1716-1740.

**Brasiliano, A.; Souza, W.R.; Doz,G.N.; Brito, J.L.V.** (2008): A Study of Damage Identification and Crack Propagation in Concrete Beams. *Structural Durability and Health Monitoring* Vol. 4, No. 2, pp. 53-66.

**Chakraborty, A.; Gopalakrishnan, S.** (2005): A spectrally formulated plate element for wave propagation analysis in anisotropic material. *Computer Methods in Applied Mechanics and Engineering*, vol. 194, pp. 4425-4446.

**Chang, C.C.; Chen, L.W.** (2005): Detection of the location and size of cracks in the multiple cracked beam by spatial wavelet-based approach. *Mechanical Systems and Signal Processing*, vol.19, pp. 139-155.

**Chakraborty, A.; Gopalakrishnan, S.** (2004): Wave propagation in inhomogeneous layered media: Solution of forward and inverse problems. *Acta Mechanica*, vol. 169, pp. 153-185.

**Chasalevris, A.C.; Papadopoulos, C.A.**(2006): Identification of multiple cracks in beams under bending. *Mechanical Systems and Signal Processing* 20 (7), pp. 1631-1673.

**Chen, X.F.; Zi, Y.Y.; Li, B.; He, Z.J.** (2006): Identification of multiple cracks using a dynamic mesh-refinement method. *The Journal of Strain Analysis for Engineering Design* 41 (1), pp. 31-39.

**Cornwell, P.; Doebling, S. W.; Farrar, C. R.** (1999): Application of the Strain Energy Damage Detection Method to Plate-like Structures. *J Sound and Vibration*, vol. 224, no. 2, pp. 359-374.

**Daubechis, I.** (1992): Ten lectures on wavelets. CBMS-NSF Series in Applied Mathematics. Philadelphia, SIAM.

**Davis, P. J.** (1963): Interpolation and Approximation. Blaisdell, New York.

**Doebling, S.W.; Farrar, C.; Prime, M.B.; Daniel, W.S.** (1996): Damage Identification and Health Monitoring of Structural and Mechanical Systems from Changes in their Vibration Characteristics: A Literature Review, LA-13070-MS.

**Doyle, J.F.** (1999): Wave propagation in structures. New York, Springer.

**Feng, Yanhui A.; Schlindweina, Fernando S.** (2009): Normalized wavelet packets quantifiers for condition monitoring. *Mechanical Systems and Signal Processing* Vol. 23, No. 3, Pages 712-723.

**Gangadharan, R.; RoyMahapatra, D.; Gopalakrishnan. S; Murthy, C.R.L.;**

**Bhat, M.R.**(2009): On the sensitivity of elastic waves due to structural damages: Time-frequency based indexing method *Journal of Sound and Vibration* vol. 320, 915-941.

**Giridhara, G.; Gopalakrishnan, S.; Ruzzene, M.; Hanagud, S.; Sharma, V.K.** (2007): Frequency Domain based Damage Index for Structural Health Monitoring using Laser Vibrometry. $48^{th}$ AIAA/ASME/ASCE/AHS/ASC Structures, Structural Dynamics, and Materials conference, Hawaii.

**Gopalakrishnan, S. Chakraborty, A; Mahapatra, D.R.** (2007): Spectral Finite Element Method: Wave Propagation,Diagnostics and Control in Anisotropic and Inhomogeneous Structures, Springer,Berlin.

**Gupta, priyabnk; Giridhara, G.;Gopalakrishnan, S.** (2008): Damage Detection based on Damage Force indicator using Reduced-Order FE models. *International Journal for Computational Methods in Engineering Science and Mechanics*, vol. 9, no. 3, pp. 154-170.

**Ho, Y.K.; Ewins, D.J.** (1999): Numerical Evaluation of the Damage Index. Structural Health Monitoring 2000. Stanford University, Palo Alto, California, pp. 995-1011.

**Horst, P.** (2005): Criteria for the Assessment of Multiple Site Damage in Ageing Aircraft. *Structural Durability and Health Monitoring* ,Vol. 1, No. 1, pp. 49-66.

**Kanchi Venkatesulu Reddy; Ranjan Ganguli** (2007): Fourier Analysis of Mode Shapes of Damaged Beams. *CMC: Computers, Materials and Continua* , Vol. 5, No. 2, pp. 79-98.

**Kim, J.T.; Stubbs, N.** (2003): Crack Detection in Beam Type Structures Using FrequencynData. *J Sound and Vibration* , vol. 259,no. ,pp. 145-160.

**Lee, Jungwhee; Kim, Sungkon** (2007): Structural Damage Detection in the Frequency Domain using Neural Networks. *Journal of Intelligent Material Systems and Structures*, Vol. 18, No. 8, 785-792.

**Lestari, W.** (2001): Damage of Composite Structures: Detection Technique, Dynamic Response and Residual Strength. Ph.D Thesis, Georgia Institute of Technology, Atlanta, USA.

**Li, Y.Y.; Cheng, L.; Yam, L.H.; Wong, W.O.** (2002): Identification of damage locations for plate-like structures using damage sensitive indices: strain modal approach. *Computer and Structures*, vol. 80,no.25, pp.1881-1894.

**Luo H.; Hanagud S.** (1997): An integral Equation for Changes in the Structural Dynamics Characteristics of Undamaged Structures. *Int J Solids Struct*, 34(35-36), pp. 4557-4579.

**Mitra, M., Goplakrishnan, S.** (2008): Wave propagation analysis in anisotropic

plate using Wavelet Spectral Element approach. *ASME Journal of Applied Mechanics*, Vol. 75, pp. 014504.

**Mitra, M.; Goplakrishnan S.** (2006): Extraction of wave characteristics from wavelet based spectral finite element formulation. *Mechanical Systems and Signal processing*, vol. 20, pp. 2046-2079.

**Mitra, M.; Goplakrishnan S.** (2006): Wavelet based 2-D Spectral Finite Element Formulation for Wave Propagation Analysis in Isotropic Plates. *CMES: Computer Modeling in Engineering and Science*, vol. 1, no. 1, pp. 11-29.

**Mitra, M.; Goplakrishnan S.** (2006): Wavelet based spectral finite element modeling and detection of de-lamination in composite beams. *Proceedings of Royal Society A*, vol. 462, no. 2070, pp. 1721-1740.

**Mitra, M.; Goplakrishnan S.** (2006): Wave propagation analysis in carbon nanotube embedded composite using wavelet based spectral finite element. *Smart Materials and Structures*, vol. 15, pp. 104-122.

**Mitra, M.; Goplakrishnan S.** (2005): Spectrally Formulated Wavelet Finite Element for Wave propagation and Impact Force Identification in Connected 1-D Waveguides. *International Journal of Solids and Structures*, vol. 42, pp. 4695-4721.

**Nag, A.; Roy Mahapatra, D.; Gopalakrishnan, S.** (2002): Identification of Delamination in Composite Beam using a Damaged Spectral Element. *Struct Health Monitoring*, vol. 1, no. 1,pp. 105-126.

**Nayeh, A.H.; Pai, P.F.** (2004): Linear and Nonlinear Structural Analysis. New Jersey, John Wiley.

**Ostachowicz, W.M.** (2008): Damage detection of structures using spectral finite element method, *Computers and Structures* vol. 86, pp. 454-462.

**Pandey, A.K.; Biswas, M.; Samman, M.M.** (1991): Damage Detection from Changes in Curvature Mode Shapes. *J Sound and Vibration*, vol.145,no.2, pp.321-332.

**Patton, R.D.; Marks, P.C.** (1996): One dimensional finite elements based on the Daubechies family of wavelets. *AIAA Journal*, vol. 34, pp. 1696-1698.

**Peng,Z.K.; Chu, F.L.** (2004): Application of the wavelet transform in machine condition monitoring and fault diagnostics: a review with bibliography, *Mechanical Systems and Signal Processing*, Vol. 18, No. 2, pp. 199-221.

**Prabhakar,S.; Sekhar, A.S.; Mohanty, A.R.** (2001): Detection and monitoring of cracks in a rotor-bearing system using wavelet transforms. *Journal of the Mechanical Systems and Signal Processing*. Vol. 15(2), pp. 447-450.

**Raghuprasad, A.B.K.; Lakshmanan, N.; Gopalakrishnan, N.; Muthumani, K.**

(2008): Sensitivity of Eigen Value to Damage and Its Identification. *Structural Durability and Health Monitoring* , Vol. 4, No. 3, pp. 117-144.

**Ramana M. Pidaparti; Evan J. Neblett** (2007): Neural Network Mapping of Corrosion Induced Chemical Elements Degradation in Aircraft Aluminum. *CMC: Computers, Materials and Continua* , Vol. 5, No. 1, pp. 1-10.

**Ramana M. Pidaparti** (2006): Aircraft Structural Integrity Assessment through Computational Intelligence Techniques. *Structural Durability and Health Monitoring* , Vol. 2, No. 3, pp. 131-148.

**Schulz, M.J.; Naser, A.S.; Pai, P.F.; Chung, J.** (1998): Locating structural damage using frequency response reference functions. *Journal of Intelligent Material Systems and Structures*, vol. 9, pp. 899-905.

**Sekhar, A.S.**(2008): Multiple cracks effects and identification. *Mechanical Systems and Signal Processing*, vol. 22, pp. 845-878.

**Shamsh Tabrez; Mira Mitra; S. Gopalakrishnan** (2007) Modeling of Degraded Composite Beam Due to Moisture Absorption For Wave Based Detection. *Computer Modeling in Engineering and Sciences*, Vol. 22, No. 1, pp. 77-90

**Sharma, V.K.; Ruzzene, M.; Hanagud, S.** (2006): Perturbation Analysis of Damaged Plates. *Int J Solids Struct*, vol. 43, no. 16, pp. 4648-4672.

**Sharma, V.K.; Ruzzene, M.; Hanagud, S.** (2006): Damage Index Estimation in Beams and Plates Using Laser Vibrometry. *AIAA J*, vol. 44, pp. 919-923.

**Shi, Z.Y.; Law, S.S.; Zhang, L.M.** (1998): Structural damage localization from modal strain energy change. *Journal of Sound and Vibration*, vol. 218, no. 5, pp. 825-844.

**Sohn, H.; Farrar, C.R.; Hemez, F.M.; Shunk, D.D.; Stinemates, D.W.; Nadler, B.R.** (2003): A Review of Structural Health Monitoring Literature: 1996-2001. Technical Report LA-13976-MS. Los Alamos National Laboratory, Los Alamos, NM.

**Sreekanth Kumar, D.; Roy Mahapatra, D.; Gopalakrishnan, S.** (2004): A Spectral Finite Element for wave propagation and Structural Diagnostic Analysis in a Composite beam with Transverse Cracks. *Finite Elements in Analysis and Design*, vol, 40, pp. 1729-1751.

**Staszewski, W.J.; Boller, C.; Tomlinson, G.** (2003) *Health Monitoring of Aerospace Structures-Smart Sensors and Signal Processing*. Chichester, UK, John Wiley and Sons .

**Williams, J.R.; Amaratunga, K.** (1997): A Discrete wavelet transform without edge effects using wavelet extrapolation. *Journal of Fourier Analysis and Applications*, vol.3, pp. 435-449.

**Williams, J.R.; Amaratunga, K.** (1994): Introduction to wavelets in engineering. *International Journal for Numerical Methods in Engineering*, vol. 37, pp. 2365-2388.

**Xuefeng, C.; Zhengjia, H.; Qiang G.; Yanyang, Z.** (2005): Identification of crack damage with wavelet finite element, *Scientific Networks Key Engineering Materials*293-294, pp. 63-69.